# REPORT DOCUMENTATION PAGE

AFRL-SR-BL-TR-99-

0028



| 1. AGENCY USE ONLY *(Leave blank)* | 2. REPORT DATE | 3. REPORT TYPE AND DATES COVERED |
|---|---|---|
| | January 1999 | Final Technical Report 1 May 97 to 30 Jun 98 |

**4. TITLE AND SUBTITLE**
"Round Robin Measurements of Mechanical Properties of MEMS"

**5. FUNDING NUMBERS**
F49620-97-1-0324
2302/DS

**6. AUTHOR(S)**
Wolfgang G. Knauss
Ioannis Chasiotis

**7. PERFORMING ORGANIZATION NAME(S) AND ADDRESS(ES)**
California Institute of Technology
Graduate Aeronautical Laboratories
1200 East California Boulevard
Pasadena, CA 91125

**8. PERFORMING ORGANIZATION REPORT NUMBER**
SM 98-12
CIT 63503

**9. SPONSORING/MONITORING AGENCY NAME(S) AND ADDRESS(ES)**
AFOSR/NA
801 N. Randolph Street, Rm 732
Arlington, VA 22203-1977

**10. SPONSORING/MONITORING AGENCY REPORT NUMBER**
F49620-97-1-0324

**11. SUPPLEMENTARY NOTES**
Substantial portions have been published in Microelectromechanical Structures for Materials Research, Materials Research Society, Vol. 518, pp. 57-65, 1998, entitled "Round-Robin Tests of Modulus and Strength of Polysilicon"

**12a. DISTRIBUTION AVAILABILITY STATEMENT**
Approved for public release; distribution unlimited.

**12b. DISTRIBUTION CODE**

19990209 086

**13. ABSTRACT** *(Maximum 200 words)*

A new method for tensile testing of thin fume has been developed. The method employs AFM or STM acquired surface topologies of deforming specimens to determine (fields of) strains. An electrostatic grip apparatus was designed and implemented to measure the elastic and failure properties (Young's modulus, Poisson's ratio, tensile strength) of surface micromachined polysilicon specimens. The tensile specimens were "dog-bone" shaped ending in a large 'paddle' for electrostatic gripping. The deformation of a part of the test section is monitored by an Atomic Force Microscope (AFM). The topographic records of the specimen surface, obtained during the deformation, via Digital Image Correlation (DIG) method provide fields of strain. The natural surface features serve as distributed markers that depict the displacement field. An alternative operation mode, which employs tour thin gold markers to define a square area, as the base length of "micro-gages". In this mode the AFM determines the length changes between the markers. The effect of other parameters on property measurements, such as surface roughness, has been examined computationally. Results of elastic modulus values and fracture strength of small specimens are reported and compared to the results obtained by other researchers.

| 14. SUBJECT TERMS | 15. NUMBER OF PAGES |
|---|---|
| MEMS, MODULUS, NANOMECHANICS | 19 |
| | 16. PRICE CODE |

| 17. SECURITY CLASSIFICATION OF REPORT | 18. SECURITY CLASSIFICATION OF THIS PAGE | 19. SECURITY CLASSIFICATION OF ABSTRACT | 20. LIMITATION OF ABSTRACT |
|---|---|---|---|
| UNCLASSIFIED | UNCLASSIFIED | UNCLASSIFIED | UL |

CALIFORNIA INSTITUTE OF TECHNOLOGY

GRADUATE AERONAUTICAL LABORATORIES

Final Report to the

Airforce Office of Scientific Research

Grant No. F49620-97-1-0324

# "Round Robin Measurements of Mechanical Properties of MEMS"

Wolfgang G. Knauss

Ioannis Chasiotis[1]



Pasadena, January 1999

[1] Professor of Aeronautics and Applied Mechanics, and Graduate Student, respectively.

# ABSTRACT

A new method for tensile testing of thin films has been developed. The method employs AFM or STM acquired surface topologies of deforming specimens to determine (fields of) strains. An electrostatic grip apparatus was designed and implemented to measure the elastic and failure properties (Young's modulus, Poisson's ratio, tensile strength) of surface micromachined polysilicon specimens. The tensile specimens were "dog-bone" shaped ending in a large 'paddle' for electrostatic gripping.

According to the method, the deformation of a part of the test section is monitored by an Atomic Force Microscope (AFM). The topographic records of the specimen surface, obtained by the AFM during the deformation, by virtue of the Digital Image Correlation (DIC) method provide fields of strain. The natural surface features serve as distributed markers that depict the displacement field. An alternative operation mode, with larger length base, has been studied. This method employs four thin gold markers to define a square area, opposing sides of which serve to demark the base length of "micro-strain gages". In this mode of operation the AFM is used to determine the length changes between the markers. The effect of other parameters on property measurements, such as surface roughness, has been examined computationally.

This report summarizes the work that has been done and the achievements in overcoming the problems during the development of the method. Results of elastic modulus values and fracture strength of small specimens are reported and compared to the results obtained by other researchers.

# SCOPE

The following is a progress report on the "Round-Robin" experimental determination of physical properties of polysilicon specimens at the micron scale. Because of a considerable range of uncertainties in the determination of physical properties at the micron and nano-scales the objective of the present project was to perform a comparative study of modulus and possibly fracture behavior of polysilicon specimens by means of different experimental methods. Participants in this effort were Prof. W.N. Sharpe [Johns Hopkins University], S. Brown [Failure Analysis Associates] and Prof. G.C Johnson [U.C Berkeley]. These participants had measurement experience in this special domain and had performed testing with equipment available or under construction, as well as experience with specimen design and preparation through Microelectronics Center of North Carolina (MCNC). While submicron experimentation was not new to us, this present effort was new with regard to the construction of new gripping technology for the small specimens and new with respect to design and handling of fragile specimens.

This is a final report of the progress that we made in developing the method and the results that have been obtained pursuing the objective of our research. A comparison of the results that have been reported by the other participants is also provided.

## 1. Introduction

Polysilicon is the main structural material used in a wide variety of Microelectromechanical Systems (MEMS) fabricated by surface micromachining. Numerous applications [1] of this technology with significant commercial impact have been developed in the form of sensors or actuators during the last ten years. The most common ones are micromotors, microgears, microvalves, springs, diaphragms, angular and resonant accelerometers, vibratory rate gyroscopes and many others. The reliability of MEMS devices is a major issue and it can only be addressed by direct measurements on small specimens with dimensions on the same order of magnitude as the fabricated microdevices. Such properties depend on the manufacture and process conditions, deposition temperature, doping, annealing, chemical etching *etc.*

Various techniques [2]-[17] have been developed in the past to address the issues of mechanical integrity and evaluation of the mechanical properties of polysilicon. Methods such as load-deflection, beam bending, tensile and nanoidentation tests, resonant frequency measurements of microcantilever beams have provided a span of values for the elastic constants of polysilicon. An important reason for the variety of given results is the large differences in the specimen geometry. The load deflection method requires the knowledge of Poisson's ratio to evaluate Young's modulus and does not apply to compressively stressed films. Moreover, since Poisson's ratio is unknown, the errors caused by assuming a value are magnified in evaluating Young's modulus. For example, for calculating the bending moment in beam bending tests two contributions must be taken into account; the rotation of the cantilever support point due to the applied force and the moment due to the stress gradient through the thickness of the cantilever. For this method the precise knowledge of the film thickness is mandatory to evaluate accurately the mechanical constants. In this context, surface roughness plays a potentially important role and, as will be shown later, contributes to the overall error.

Tensile tests, however, are less vulnerable to errors in geometry and are more reliable from an error analysis point of view. Tensile tests have been performed using either electrostatics to grip the specimens, adhesive media, or micromanipulators and specially designed specimens in a scanning electron microscope (SEM), or using interferometry to measure displacements. In the present technique [18], direct measurements on the specimen surface can be obtained with even atomic resolution. Also from the point of view of error analysis, tensile testing is the best way to measure the elastic modulus. In the present work, elastic modulus and fracture strength values are presented, along with computational work to evaluate several parameters. The load-displacement curve has been obtained and by measuring the load cell stiffness and using a linear spring model for the setup and the modeled specimen, the elastic modulus has been calculated.

## 2. Experimental Work

**Test set-up:** At first, the arrangement for subjecting small "dog-bone" shaped specimens to tension for determining their mechanical properties is discussed. The experimental configuration, shown in fig. 1, is comprised of

(1) a miniature load cell with an accuracy of 0.15% of full scale,
(2) a step motor to induce displacements to the specimen having a minimum step of 4nm, and
(3) a y-z translation stage for proper positioning of the sample. The deformations of the specimen surface, according to the method, are monitored by means of an Atomic Force Microscope (AFM is not shown in figure 1).

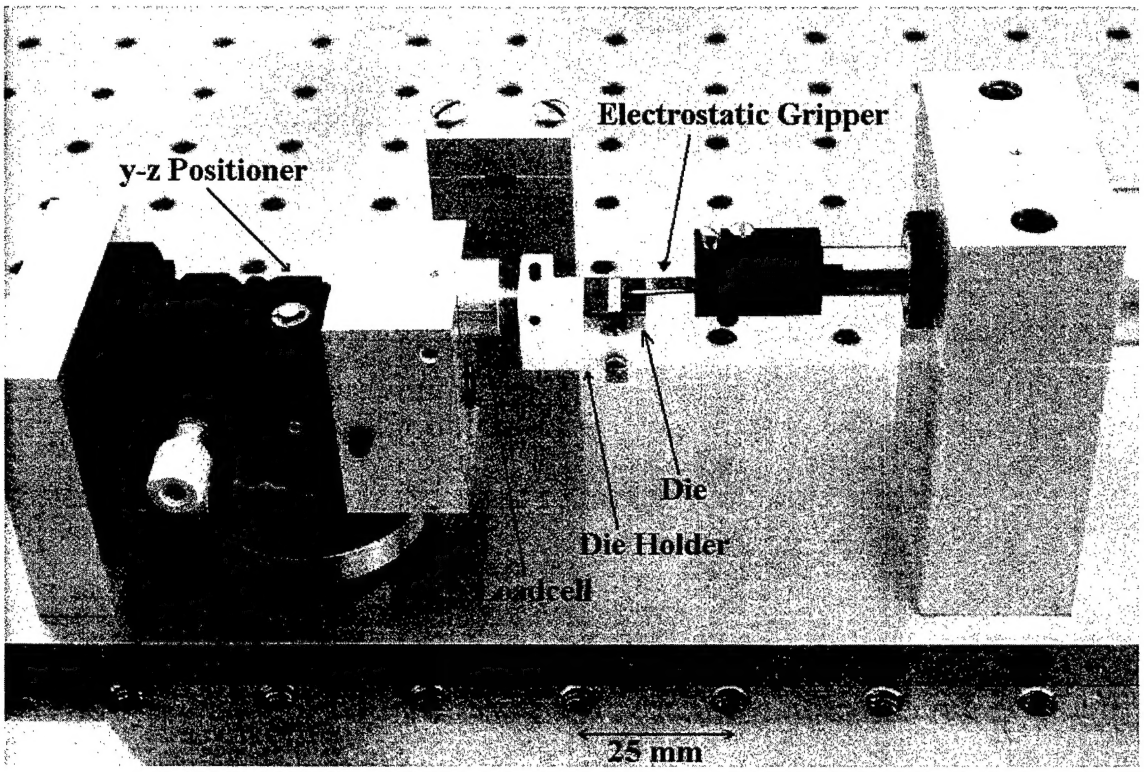


Fig. 1 The experimental setup designed for the tensile test

The experimental device has been designed to address several issues such as

(a) specimen mounting,
(b) electrical connection facilitation,
(c) load cell and specimen alignment, and
(d) proper fitting under the Atomic Force Microscope (AFM).

The performance of the components regarding their accuracy was satisfactory. The hysterisis and linearity of the load cell have been evaluated to identify possible sources of error. The linearity for the loading part was very good for our purpose (error 0.10 %). The hysterisis of the load cell has also been examined. Its effective value was on the order of 1.8%, restricted only in the low load region, and it was constant and consistent over a series of measurements. The inchworm (step motor) actuator has also been calibrated and it ran with the aid of a controller that is triggered and controlled by a personal computer. The resolution of the y-z translation stage was on the order of 1 micron; this was a satisfactory value so that proper positioning of the grip could be achieved as closely as possible to the specimen surface before applying voltage. This capability prevented any bending of the specimen during the test.

The electrical forces appeared to be sufficiently high to grip the specimen by applying a potential of 10-20 Volts (since only the paddle's weight had to be overcome). The electrostatic grip was coated by a 200nm $Si_3N_4$ insulating layer and it was fabricated at the Electrical Engineering Department here at Cal Tech. The very thin electrical insulation layer made the necessary operational voltage relatively low.

The accuracy of AFM has been tested in order to obtain a measure of the repeatability of the data. The Non-Contact Mode (NCM) was found to be a more accurate method than contact mode (AFM) for testing the specific type of thin film specimens, since vibrations may occur during the scan. On the other hand non-contact AFM is in general more suitable for surfaces that can easily develop a static charges.

**Digital Image Correlation Method (DIC):** As mentioned before, according to the method, the Digital Image Correlation (DIC) [19]-[23] method is employed to resolve strains through an interpolation scheme. This method of extracting in-plane deformations requires the ability to follow shape changes by comparing (surface) records before and after deformation. This information is obtained by a probe microscope (AFM) through records of surface features taken before and after deformation, and then computing from this information the movement of the (three-dimensional) surface features. Digital Image Correlation achieves this by defining a correlation coefficient as a function of the kinematic transformation relating the deformed to the undeformed geometry. The strains and displacements are parameters in this mapping, and are determined by a (nonlinear, multi-degree of freedom) optimization of the correlation coefficient. The method is capable of detecting displacements with a resolution of about 1/8 of a pixel, which implies the capability of resolution strains on the order 0.03% - 0.05%.

**Specimen geometry:** Tensile, bone-shaped specimens with test section dimensions of 400x80x2 microns and 400x50x2 microns, attached to a silicon die, have been designed. They were free standing beams ending in a large "paddle" for electrostatic gripping (see figure 2). The deformation of the test section area is monitored by an Atomic Force Microscope (AFM) in two modes of operation. The first employs four thin gold markers 20μm x 5μm to define a square area (fig. 3), opposing sides of which serve as base length markers of "micro-strain gages". The second mode of operation does not employ such markings, but, by way of the method of Digital Image Correlation (DIC), makes use of the natural surface roughness features as distributed markers. In this operation mode the base length for strain determination is considerably smaller. An analysis that has been performed, however, has shown that the markers introduce distortions to the displacement field. Debonding of the thin markers has also been observed. These observations lead to the use of the second mode of operation. Two different types of specimens (with and without etch holes) were designed for two different runs at MCNC and next are referred to as MUMPs19 (without etch holes) and MUMPs21 (with etch holes) as illustrated in fig.4. As seen in fig. 4 for the left side specimen the large paddle is obviously lying on the die as it can be determined by the Newtonian fringes at the beginning of the paddle. The fact that the specimens due to their "large dimensions" and consequently their weight are on the substrate led to the stiction of the first on the substrate after the chemical release. This required special steps before testing the specimens that will be discussed later.

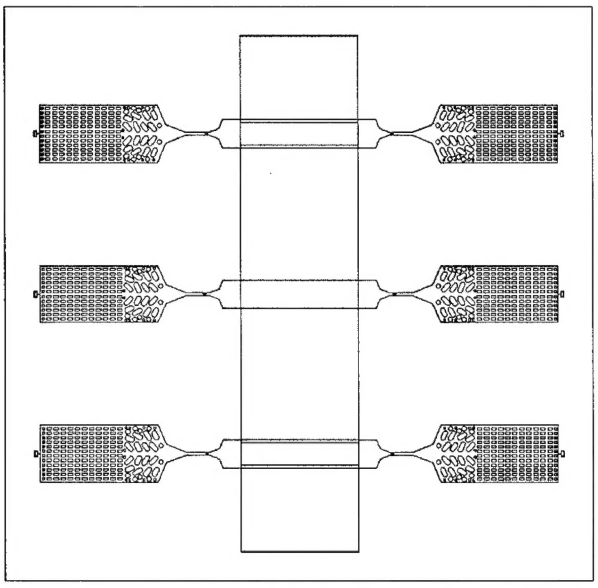

Fig. 2 Schematic of the die design carrying 6 free standing beams from MUMPs21. The dimension of the die is 1x1cm

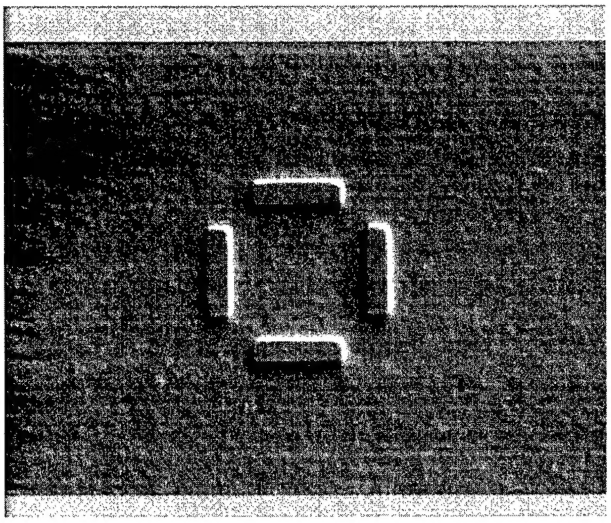

Fig. 3 The marked 20x20μm area on the specimen surface. The marks are four thin film gold bars are chrome-bonded to the surface.

The specimens for MUMPs21 were designed so as to take into account spatially frequent use of etch holes to facilitate the post-processing stage of oxide etching. The pattern for the "paddle" etch holes was chosen to avoid specimen fracture from any stress concentrations. Another point that has been addressed is the use of an "anchor" for the large and wide grip section. This ensures fracture-free handling before testing and decreases the risk of (potentially disastrous) specimen drift on the silicon die during the releasing process. A special probe stage has been built to release the paddle from the anchor by cutting the narrow beam that serves as an anchor.

**Specimen manufacture process:** The Multi-User MEMS Process (MUMP) has been used to manufacture the specimens. It is a surface micromachining process that uses three polysilicon layers as structural layers. A silicon wafer with (100) orientation, heavily doped with phosphorus using $POCl_3$ was used as the substrate. A 600nm electrical insulation layer of low-stress silicon nitride layer, deposited by low pressure chemical vapor deposition (LPCVD) followed. This layer was for the structures a hard insulation from the substrate. Then the first (nonstructural) layer of polysilicon was deposited for 500nm by LPCVD and photolithographically patterned by exposing a photoresistive material with the appropriate mask. The photoresist was etched away by a Reactive Ion Etching (RIE). This was followed by a 2.0μm phosphosilicate glass (PSG) LPCVD deposition. The latter is a sacrificial layer and by being lithographically patterned, can provide dimples under the next polysilicon film.

A mask was used to etch holes in the PSG and provide anchor holes to be filled by the subsequent polysilicon layer. Then a 2.0μm thick polysilicon structural layer was deposited followed by a 200nm PSG layer and annealing at 1050°C for 1 hour. This provided uniform doping to the middle polysilicon layer and reduced the residual stresses in the structural layer. The latter and the PSG masking layer were lithographically patterned using a mask to define the structures built by the first structural layer. Then the PSG layer was etched and used as a resistant hard mask to the etchant for the subsequent polysilicon etch providing more accurate patterning. This hard oxide mask was removed by RIE after the polysilicon has been etched. Finally, for the marker metalization the wafer is patterned lithographically with a mask and a 0.5μm metal layer of gold with a thin chrome adhesion layer, was deposited and patterned. The photoresist and the unwanted metal were then removed in a solvent bath. The release of the structures was performed by immersing the wafer in a bath of 49% HF for a sufficient amount of time that depends on the size of the structures and the density of the etch holes. This was followed by rinsing with de-ionized water and then alcohol to reduce stiction. Then the dies ware baked for 10 minutes at 110°C. The optional $CO_2$ supercritical process was used instead of the last step of baking the wafer for the MUMPs21 structures, in order to further reduce the stiction danger.

**Specimen release:** Specimens were received from MCNC in the released form (free standing specimens, fixed at one end and held at the other by way of an "anchor"). When the first batch arrive from MUMPs21, the structures turned out to be only partially released after (MCNC determined) 9.5 minutes of etching and thus an additional releasing process needed to be performed here at Caltech. Unfortunately, this resulted in fracture of the specimens and this was a major reason that caused delay to our work. We determined the proper etching time to be 10.5 minutes and a new batch of specimens has been received recently from MCNC with the newly determined release time employing the supercritical $CO_2$ process to eliminate the problem of "stiction".

At first, specimens from MUMPs19, successfully released at Caltech, were subjected to tests that revealed the problem of "stiction". The release time needed in addition to the 2.5 minutes of incomplete release performed by MCNC, was an other 13.5 minutes in 49% HF with 15 minutes rinsing in water, 35 minutes post treatment in methanol in order to minimize stiction, and 5 minutes of baking. During the release in the water and subsequently in alcohol, the polysilicon cantilever beams curved strongly up but finally they remained stuck down to the die surface (stiction effect). The temporary bending is attributed to the high compressive stresses, due to the prior deposition on silicon oxide and the thermal expansion coefficient mismatch.

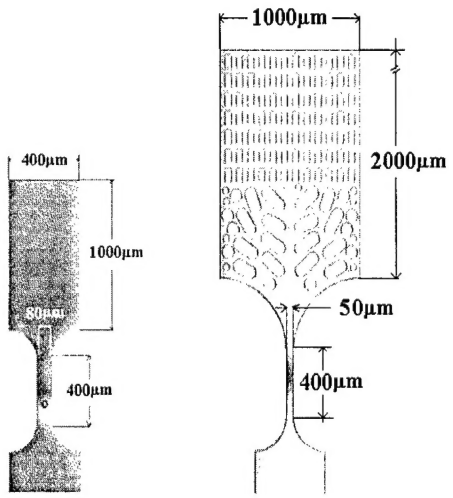


Fig. 4. Detail and dimensions of the tensile specimens designed on silicon chip. The thickness of the specimens is 2 μm.

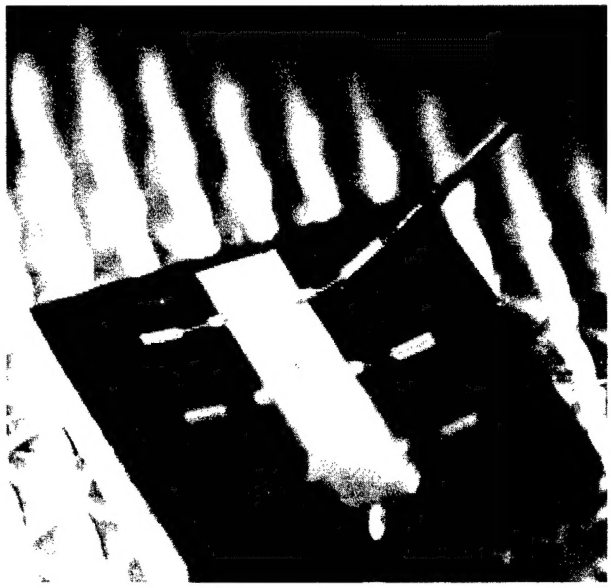

Fig. 5 The stiction problem appeared to be an important issue; release was accomplished by mechanically probing and forcing the specimen paddle end from the support.

The electrostatic forces applied to lift the specimen paddle and bring it in contact with the grip proved to be inefficient to overcome the stiction forces. Although these forces theoretically should not be that strong, they were strong enough to prevent the pull off from the die. An other way had to be determined to free the structures and this was done by probing them. In order to probe them a very sensitive, sharp and accurate probing device with very low stiffness was used, so that the movement of the tip would not fracture the specimens. The tip was manufactured using the same technique that is used to fabricate sharp tips for STM devices by subjecting a Tungsten wire into NaOH solution and applying voltage.

**Specimen surface topography:** A study of the specimen surface shows that the topography appears to be uneven with columnar grains and an average grain size of 250-350nm diameter with a height distribution ranging from 200nm to 400nm (fig. 6). The topography varies with grains emerging up to 30nm above the average level of the surface. These are certainly parameters that have to be taken into account when the experimental results are evaluated. A computational analysis of the effects of these features has been done, providing a better interpretation of the experimental data.

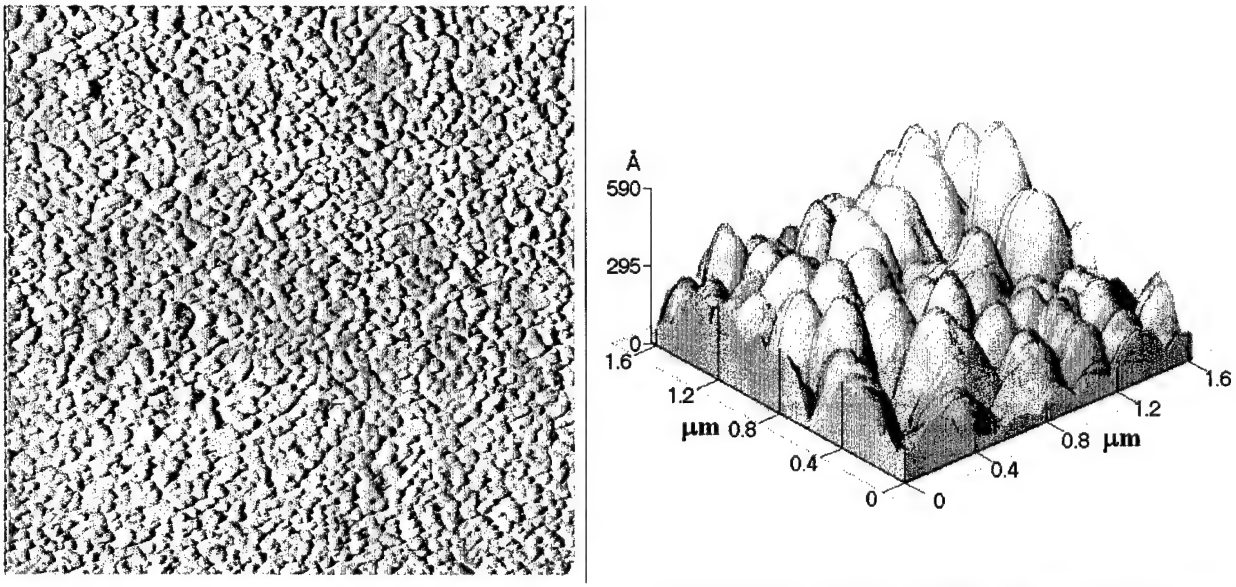


Fig. 6 Left: Grain size distribution in a 20 micron x 20 micron region. Right: Three-dimensional rendering of the surface topography of a 1.6µm x 1.6µm region revealing the columnar structure of the material and the surface non-uniformity. The z-direction is exaggerated compared to the lateral dimensions to make the grain structure more apparent. The maximum value on the z-axis is the local maximum height value. The image was obtained using an AFM in the Contact Mode.

**Film thickness measurements:** The AFM is capable of providing images with atomic resolution. This assures that AFM measurements provide an accurate value of the film thickness, provided the latter is within the capability range of the microscope. The thickness that was so measured for MUMPs19 polysilicon was 1895nm with a std. deviation of 50 nm, compared to the value given by MCNC (using a different method) of 1965nm, with a std. deviation of 48nm. The AFM value agrees also with the value obtained by means of an SEM (1880nm). The thickness that was measured for MUMPs21 for polysilicon was 1915nm with a std. deviation 40nm, compared to the given value of 1926nm, with a std. deviation of 42nm. Basically the standard deviation corresponds to the surface roughness that has been described in the previous paragraph. The two independent measurements (by means of AFM and SEM) gave almost the same results that were used to obtain more accurate values of the elastic constants instead of using the nominal value (2μm) for the film thickness. For example, the use of the nominal value of the thickness for the case of tensile test yields a 5% error that translates into 12% for bending.

**Test Results:** After being able to release the specimens (MUMPs19) from the substrate they were tested using the electrostatic method. The specimen fracture was brittle, as expected, revealing the columnar structure of polysilicon as seen by the SEM analysis (fig. 8). However, due to the fact that the available batch of the specimens was etched twice, the fracture point was at the weak region of the specimen (fig. 7), an area that has been degraded by the long and not continuous etching time.

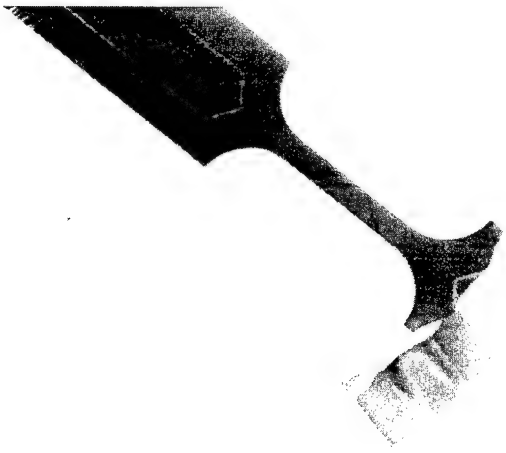

Fig. 7. Specimen fracture during test. The fracture occurred in an area that had been affected by the (necessary) secondary etching

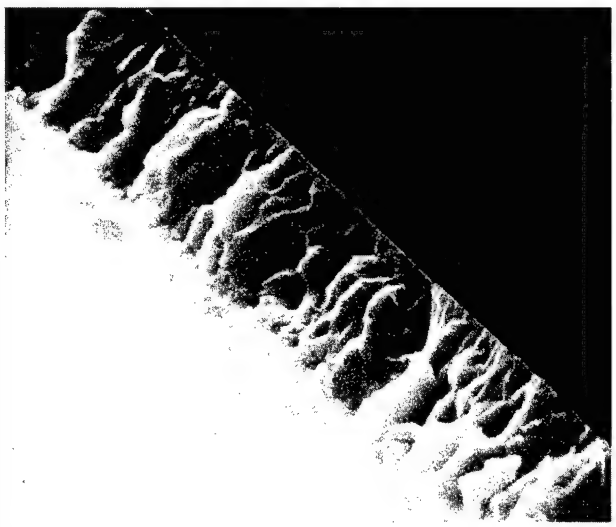

Fig. 8. SEM picture of the fractured cross section of the specimen. The columnar grain structure can be seen from the grooves and the extrusions of the fractured section.

The force-elongation behavior was found to be very linear as seen at figs. 9 & 10. The voltage used to test these structures was between 70 and 80 Volts. This voltage agreed well with the computed necessary values for testing the specimens. For lower voltage, the linear behavior was modified by steps that indicated slipping between the grip and the paddle, resulting in intermittently stable gripping. The higher voltage appeared to give a more stable behavior until fracture, since no slip occurred during that test. Higher voltage appeared to be risky in as much as it leaded to local voltage breakdown, spark formation and eventually specimen damage.

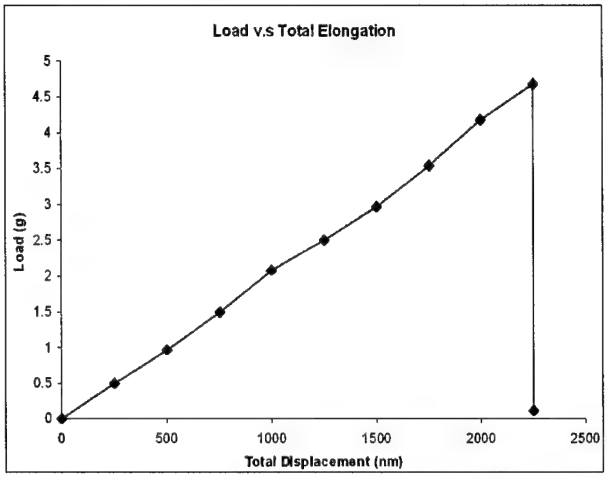


Fig. 9. Load v.s total specimen elongation.

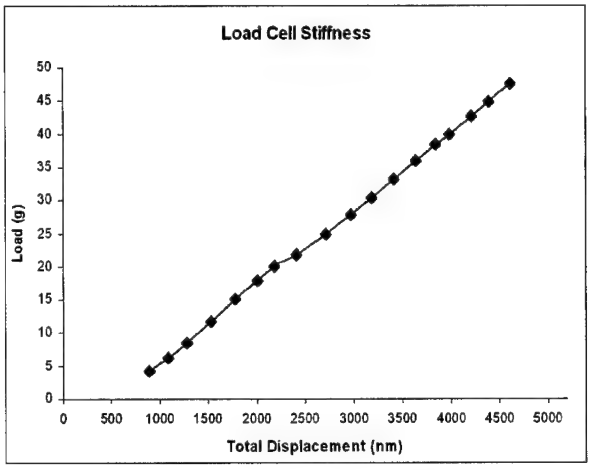


Fig. 10. Load v.s load cell elongation.

The system stiffness measured at the end of the test was mostly comprised by the stiffness of the load cell. The contribution of the rest parts of the test system to the overall compliance is small compared to that of the load cell. Then by modeling he specimen and applying the linear spring model, the modulus values that are shown in Table 1 have been obtained.

Table 1. Round Robin results

| | (MUMPs21) | | | | (MUMPs19) |
|---|---|---|---|---|---|
| | U.C Berkeley | Failure Analysis Associates | Johns Hopkins University | Caltech | Caltech |
| Thickness (microns) | 2 | 2 | 1.5 / 3.5 | 1.91 | 1.89 |
| Etch time (minutes) | 9 | 2.5 | 9 | 11.5 | 2.5 + 13.5 |
| Young's modulus (GPa) | 174 | 137 | 136/142 | **136.9** (STDV=3.2) | **132** |
| Fracture Strength (GPa) | 2.8 | 2.7 | 1.3 | **1.0** (STDV=0.1) | **0.3** |
| Friction Coefficient | N/A | N/A | N/A | **0.08 - 0.1** | N/A |

Recently, specimens from MUMPs21 have been tested after complete HF release and $CO_2$ drying. The specimens displayed no quality and surface degradation since the exposure time to

HF was considerably lower. The tensile strength of these specimens appeared much better than that from MUMPs19 specimens and close to the values reported by other Round Robin participant. Based on the measured values of force slip for which slip occurred, the static friction coefficient has also been calculated. The results are presented in Table 1 for better comparison with the results from MUMPs19 and the results of the other Round Robin participants from the same run.

The difference in the values for MUMPs19 we present was the result of the long etching time that weakened the specimens' structure [24]. The specimens of this run, as mentioned, broke at the weak region (figure 7) which was possibly thinner. The measured fracture strength was 0.3 GPa, which is a low limit for strength of the test section, and is definitely higher in reality. In conclusion we see that the value that is mostly affected by the long HF exposure was the fracture strength, as expected, since the geometric characteristics of the specimen changed displaying a non-uniform thickness. This is also apparent after comparison to the values of tensile strength that were measured for the MUMPs21 run.

## 3. Supplemental Theoretical & Computational Work

As mentioned before, we employed four thin gold markers 20 μm x 5 μm arranged in a square to define "micro-strain gages". In this mode of operation the AFM is used to determine the length changes between the markers for measuring strains in the tension and transverse directions. A finite element program was developed (using ABAQUS) to investigate the influence of the gold markers that were deposited on the specimen surface, on the stress and displacement field. The displacement field around the markers and in the surrounded area did not seem to be significantly affected by them. However they did display significant bending behavior compared to the rest of the specimen, due to the much lower elastic constant and the higher Poisson's ratio for gold (figs. 11, 12). In the contour plots, the color of the markers represents their top surface strain field and not the strains on the specimen's surface. The FEM analysis that has been performed can be used along with the strain data to accurately evaluate the strain field through application of the DIC method.

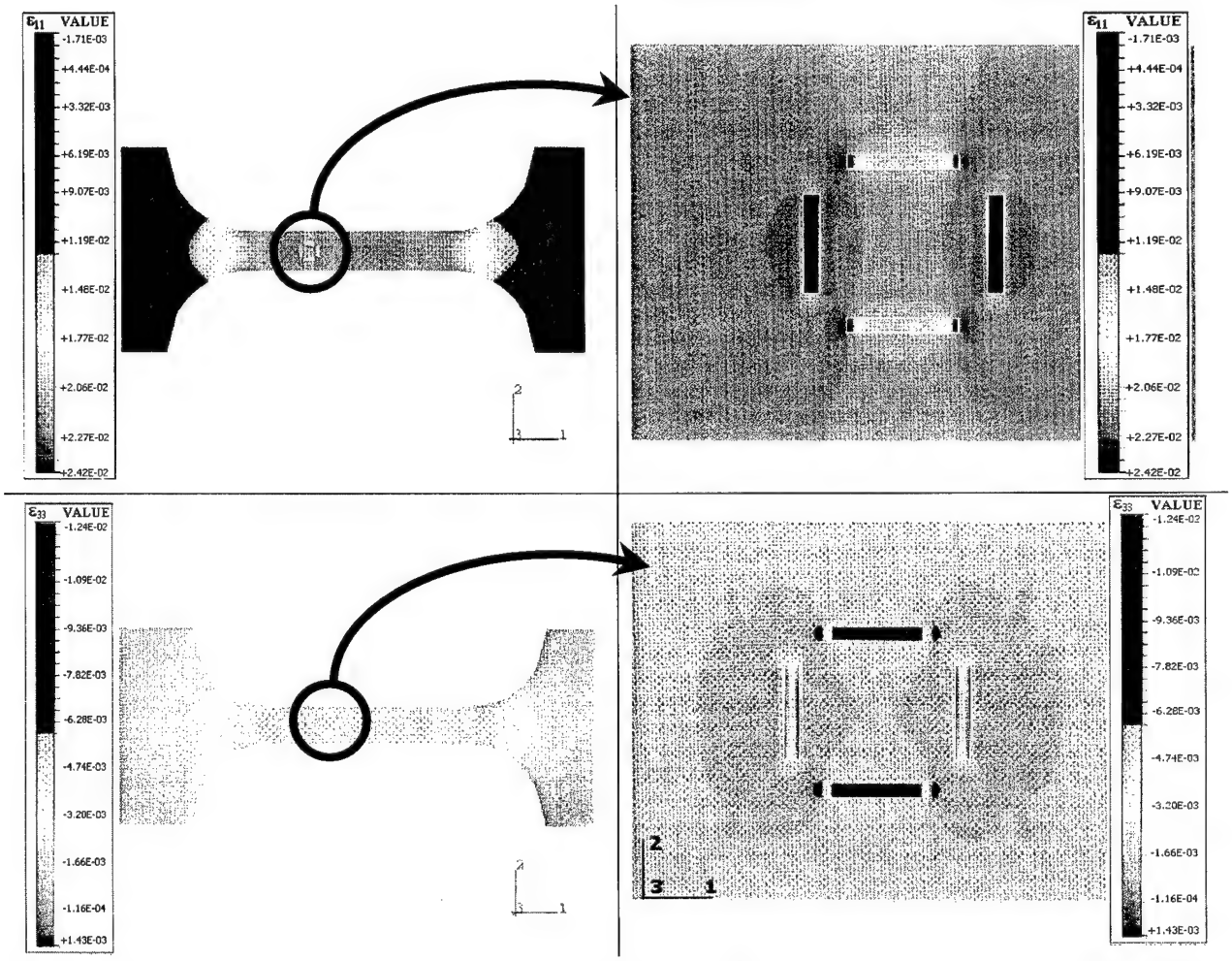


Fig. 11. $\varepsilon_{11}$ and $\varepsilon_{33}$ strain field around the gold marks. The strain fields appeared to be slightly distorted.

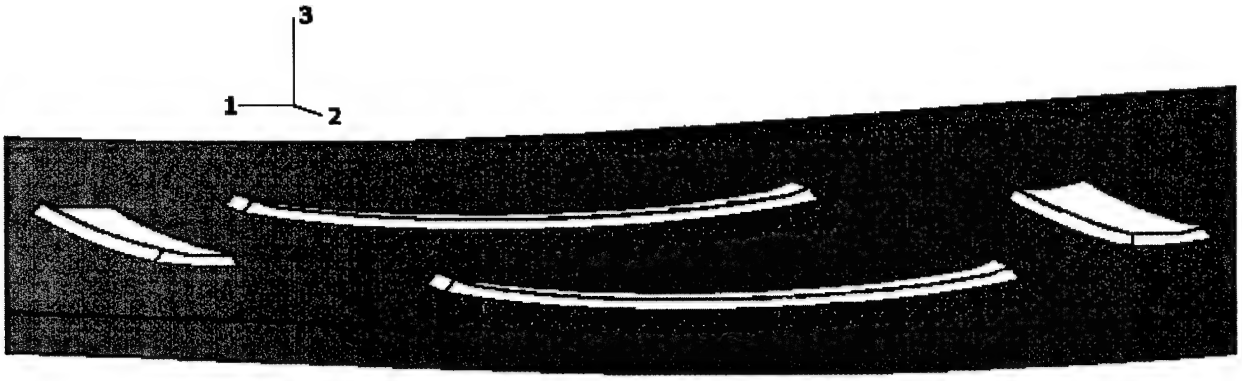


Fig. 12. The mismatch of the elastic moduli between polysilicon and gold resulted to a bending behavior of the metal markers.

**Effect of surface roughness:** A (two-dimensional) finite element program (developed also for ABAQUS) has been exercised to investigate the influence of surface roughness (bumps) as observed in the micro-manufactured specimens. A plane stress model has been used. The specimens have been manufactured using LPCVD deposition and lithographic methods that inherently cause an uneven surface topography. Usually, this feature is not taken into account when evaluating experimental results. The influence of two parameters was examined: The average bump height (wave amplitude) and the bump width (wave length) for both tensile and bending tests. The bumps have been modeled as sinusoidal surface variations, which corresponds satisfactorily to the real surface topography (see also fig. 6) of the AFM data.

The sensitivity of the data to the surface roughness is shown in figures 13 and 14 for the bending and the tension case. We hasten to point out that these results are two-dimensional, and that three-dimensional roughness would lead to wider variations. The parameter range used for the computations was larger than that usually observed, and was chosen to verify the data tendency.
In general indirect test methods are based on approximate values of the specimen thickness. This numerical analysis proved that the error due to the surface roughness of these approximations can be important, sometimes exceeding the experimental and systematic errors.

The same specimen configuration has also been used to identify the effects of the surface non-uniformity to the experimental results obtained from testing the specimens that have been subjected to bending and tensile tests in the Round Robin work. Taking into account the data provided in fig. 6 and according to the given plots in fig. 13 and fig.14, the error for the tensile test was about 1.5 %, where for the case of bending the error was almost 5%. It becomes obvious that the effect of the surface roughness to the data accuracy is stronger in the case of bending tests, reaching values of almost 10% for small grain size.

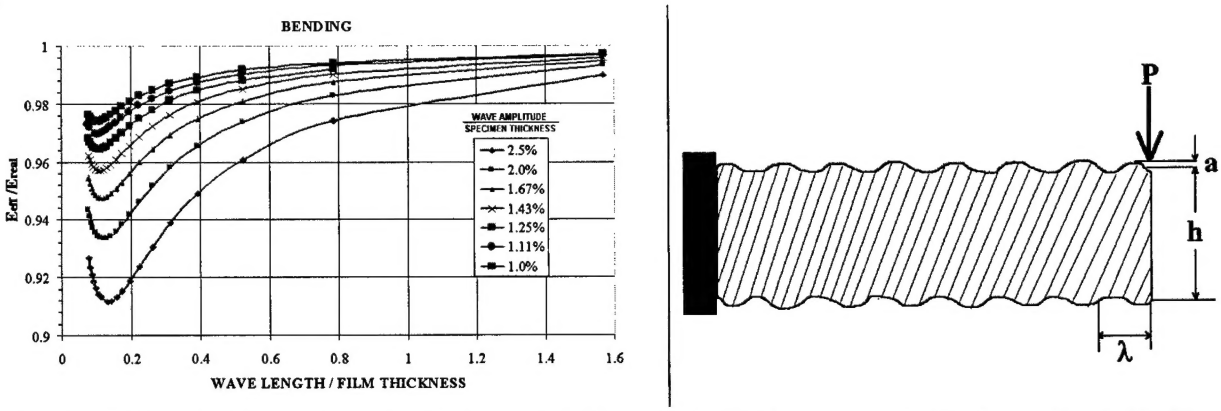


Fig. 13. Dependence of the ratio of the actual Young's Modulus to the "effective value", $E_{eff}/E_{real}$, measured in a bending test with respect to the wavelength and the amplitude of the surface bumps. Right: the profile of the geometry used for the model.

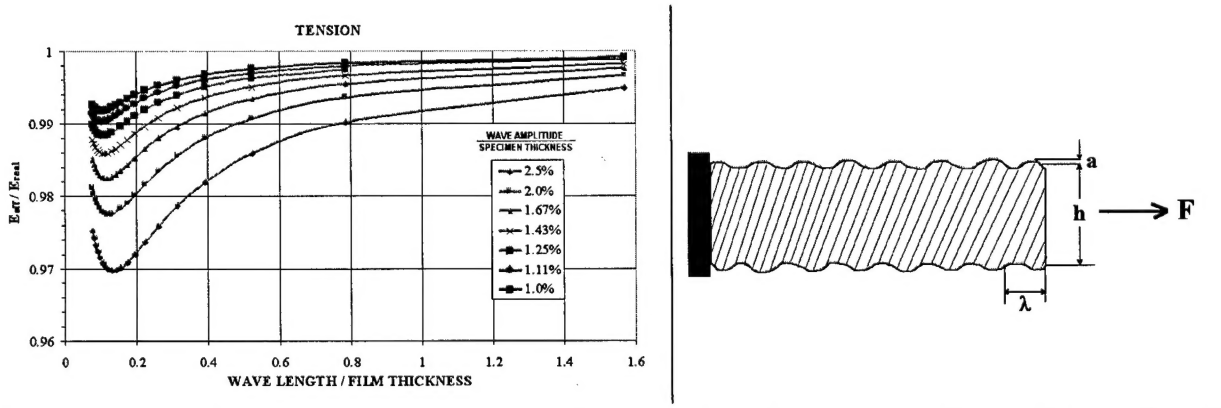


Fig. 14. Effect of surface roughness on tensile properties. Compared to figure 13 the effect is three times smaller than the effect on bending and minimal compared to other experimental errors. Right: the profile of the geometry used for the model.

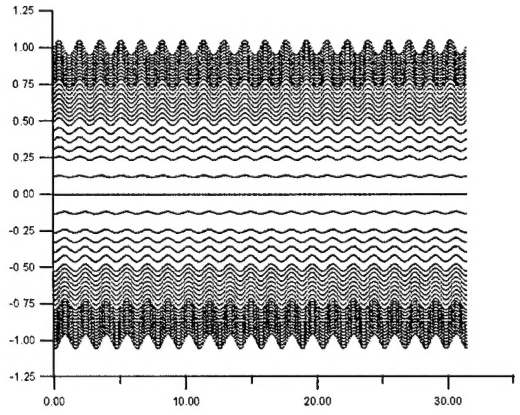

Fig. 15. The specimen model used for the FEM analysis. In this model, the bumps were simulated by a sinusoidal surface profile with uniformly decreasing amplitude towards the midplane of the specimens. This is validated by figure 6.

**Summary**

In the present work, the force-displacement response of the very small specimens has been successfully recorded. By use of a linear spring model that includes the numerical evaluation of the deformed geometry and the measured load cell compliance, the value for Young's modulus has been obtained. Following this accomplishment the second mode of operation of the AFM will be pursued to determine the strain directly from surface topography records obtained during the deformation under loading of specimens from both MUMPs19 and MUMPs21 runs and by implementing the DIC analysis. Ultimately this mode of operation is the faster and the preferred version.

## REFERENCES


1. Roger T. Howe, Bernhard E. Boser, "Polysilicon Integrated Microsystems: Technologies And Applications", Sensors and Actuators A, **56** (1996) p. 167-177.

2. P. Lange, M. Kirsten, W. Riethmuller, B. Wenk, "Thick Polycrystalline Silicon For Surface Micro-mechanical Applications: Deposition, Structuring And Mechanical Characterization", Sensors and Actuators A, **54** (1996) p. 674-678.

3. U Beerschwingerf, D Mathiesont, R Reubent, "A Study of Wear on MEMS Contact Morphologies", J. Micromech. Microeng. **4** (1994) p.95-105.

4. M. T. A. Saif and N. C. MacDonald, "Planarity of Large MEMS", J. of Micromechanical Systems, **5** (2) (1996) p. 79-97.

5. W. N. Sharpe, Jr., Bin Yuan, R. L. Edwards, "A New Technique For Measuring The Mechanical Properties Of Thin Films", J. of Micro-mechanical Systems, **6** (3) (1997) p. 193-199.

6. William N. Sharpe, Ranji Vaidyanathan, Richard L. Edwards, "Effect Of Etch Holes On The Mechanical Properties of Polysilicon", J. Vac. Science B, **15** (5) (1997) p.1599-1603.

7. William N. Sharpe, Jr. B. Yuan, R.Vaidyanathan, "Measurements Of Young's Modulus, Poisson's Ratio, And Tensile Strength Of Polysilicon".

8. Staffan Greek, Fredric Ericson, Stefan Johansson, Jan-Ake Schweitz, "In Situ Tensile Strength Measurement and Weibull Analysis Of Thick Film and Thin Film Micromachined Polysilicon Structures", Thin Solid Films, **292** (1997) p.247-254.

9. Lucas S., K Kis-Sion, J Pinel, O Bonnaud, "Polysilicon Cantilever Beam Using Surface Micromachining Technology For Anolication in Microswitches", J. Micromech. Microeng. **7** (1997) p.159-161.

10. P. French, "Development of Surface Micro-machining Compatible With On-Chip Electronics", J. Micromech. Microeng. **6** (1996) p. 197-211.

11. Bumkyoo Charity, E. G. Lovely, "Improved Analysis Of Microbeams Under Mechanical And Electrostatic Loads", J. Micromech. Microeng. **7** (1997) p.24-29.

12. J. Koskinent, J. E. Steinwall, R Soave, "Microtensile Testing Of Free-Standing Polysilicon Fibers of Various Grain Sizes", J. Micromech. Microeng. **3** (1993) p.13-17.

13. O. Tabata. K. Kawahata, S.Sugiyama, I.Igarashi, "Mechanical Property Measurements of Thin Films Using Load-Deflection of Composite Rectangular Membranes", Sensors and Actuators A, **20** (1989) p.135-141.

14. Toshiyuki Tsuchiya, Osamu Tabata, "Tensile Testing of Polycrystalline Silicon Thin Films Using Electrostatic Force Grip", T.IEE Japan, Vol **116-E** (10) (1996) p. 441-446.

15. D. Maier-Schneidert, A. Koprululu, S. Balihausen Holm, "Elastic Properties and Microstructure Of LPCVD Polysilicon Films", J. Micromech. Microeng. **6** (1996) p.436-446.

16. D. Maier-Schneidert, J Malbacht, E Obermeiert, "Variations in Young's Modulus Intrinsic Stress of PCVD-Polysilicon due to High-Temperature Annealing", J. Micromech. Microeng. **5** (1995) p.121-124.

17. Jan-Ake Schweitz, "Mechanical Characterization of Thin Films by Micromechanical Techniques", MRS Bulletin, **7** (1992) p.34-45

18. I. Chasiotis, W. G. Knauss, "Mechanical Properties of Thin Polysilicon Films by Means of Probe Microscopy", Proceedings SPIE Symposium, Santa Clara CA, 1998.

19. G. Vendroux, W. G. Knauss, "Submicron deformation field measurements II: Improved Digital Image Correlation", Experimental Mechanics **38** (2), pp. 86-92, 1998.

20. Sutton M.A., Wolters W.J., Peters W.H., Ranson W.F. and McNeil S.R., "Determination of Displacements using an Improved Digital Correlation Method," Image Vision Computing, 1 (3) 133-139 (1983).

21. Sutton M.A., Cheng M., Peters W.H., Chao Y.J. and McNeil S.R., "Application of an Optimized Digital Image Correlation Method to Planar Deformation Analysis," Image Vision Computing, 4 (3) 143-150 (1986).

22. Sutton M.A., McNeil S.R., Jang J. and Babai M., "The Effect of Subpixel Image Restauration on Digital Image Correlation Estimates," Optical Engineering, 27 (10) 870-877 (1988).

23. Luo P.F., Chao Y.J., Sutton M.A. and Peters W.H., "Accurate Measurement of Three-dimensional Deformations in Deformable and Rigid Bodies using Computer Vision," Experimental Mechanics, 33 (2) 123-132 (1993).

24. James A. Walker, Kaigham J. Gabriel, "Mechanical Integrity of Polysilicon Films Exposed To Hydrofluoric Acid Solutions", Journal of Electronic Materials, **20** (9) (1991) p. 665-670.